Journal of Advanced Joining Processes 8 (2023) 100150

Contents lists available at ScienceDirect

Journal of Advanced Joining Processes

journal homepage: www.sciencedirect.com/journal/journal-of-advanced-joining-processes

Grain size and temperature evolutions during linear friction welding of Ni-base superalloy Waspaloy: Simulations and experimental validations

Mahshad Javidikia, Morteza Sadeghifar *, Henri Champliaud, Mohammad Jahazi

Department of Mechanical Engineering, École de Technologie Supérieure, Montréal, Québec, H3C 1K3, Canada

ARTICLE INFO

Keywords:
Linear friction welding
Average grain size
Peak temperature
Finite element simulation
Optimization
Waspaloy

ABSTRACT

This research study was aimed at investigating the influence of linear friction welding parameters on grain size alteration and temperature distribution of Ni-base superalloy Waspaloy. A 3D finite element model was developed to predict average grain size and peak temperature as responses. The linear friction welding parameters consisted of oscillation amplitude, oscillation frequency, and applied pressure. Initially, the evolution of the average grain size as a function of the most influential process parameters was subsequently modeled based on the Johnson-Mehl-Avrami-Kolmogorov recrystallization model and were then validated with experimental results. Then, D-optimal design of experiments and analysis of variance were conducted to determine the most influential process parameters that affect the average grain size and peak temperature of the welded joint. Thereafter, response surface method was employed to obtain the regression models of the responses. The analysis of variance demonstrated that the P-value of the regression models was smaller than 5% and R^2, R^2_{adj}, and R^2_{Pred} were between 87% and 97%, which showed that the predictive regression models of PT and AGS can be used with a high level of confidence. The regression models were then validated by selecting two extra LFW tests in the space of the DoE. The optimum values of the welding parameters were determined to minimize the responses. The multi-criteria optimization analysis showed that both average grain size and peak temperature were more dependent on pressure than oscillation amplitude and frequency. The developed finite element and regression models can be utilized as a predictive tool for the design of joining industrial components, which minimize expensive and time-consuming experimental tests and measurements.

Introduction

Waspaloy is a Ni-base superalloy widely utilized in the aerospace industry because of its superior mechanical properties and corrosion resistance at high temperatures (Chamanfar et al., 2011; Chamanfar et al., 2013). Linear Friction Welding (LFW) is a solid-state joining operation for the production of complex components such as blade-integrated disks (Fratini et al., 2012; Bertrand et al., 2018). LFW is an emerging, high-added-value process, which has been used for the production of blade integrated disks made of titanium alloys for the compressor section of aircraft engines (Bertrand et al., 2018). The main feature of the LFW process is the small heat-affected zone as it is a solid-state joining method based on hot deformation of the two faces to be joined (Dalgård, 2011; Chamanfar, 2013). Therefore, common defects, such as porosities, segregations, and solidification cracks, usually observed in fusing welded joints, are not observed in LFW joints (Ji et al., 2016; Schroeder et al., 2012).

In the LFW process, an oscillatory motion along the weld plane and a perpendicular force to the weld plane are used to generate significant friction at the interface which results in the removal of the oxide layer and softens the material due to the frictional heat. The high temperature contact between the fresh materials on both sides of the interface combined with the applied pressure results in the formation of the joint (Dalgård, 2011; Chamanfar, 2013). Oscillation amplitude (a), oscillation frequency (f), and applied pressure (P) are the most important LFW process parameters that determine strain, strain rate, and temperature produced at the interface. The imposed thermomechanical cycle during the LFW process results in significant temperature and microstructural changes that have been reported on Aluminum alloy (Buffa et al., 2014; Buffa et al., 2017; Sivaraj et al., 2019), Titanium alloy (Bertrand et al., 2018; Ma et al., 2008; Dalgaard et al., 2009; Ma et al., 2012; McAndrew et al., 2018), Steel (Bhamji et al., 2010; Li et al., 2014; Fu et al., 2015; Li et al., 2018), and Superalloy (Chamanfar et al., 2011; Chamanfar et al., 2013; Vishwakarma et al., 2014; Chamanfar et al., 2015; Smith et al.,

* Corresponding author.
E-mail address: morteza.sadeghifar@etsmtl.ca (M. Sadeghifar).

https://doi.org/10.1016/j.jajp.2023.100150

Available online 4 July 2023

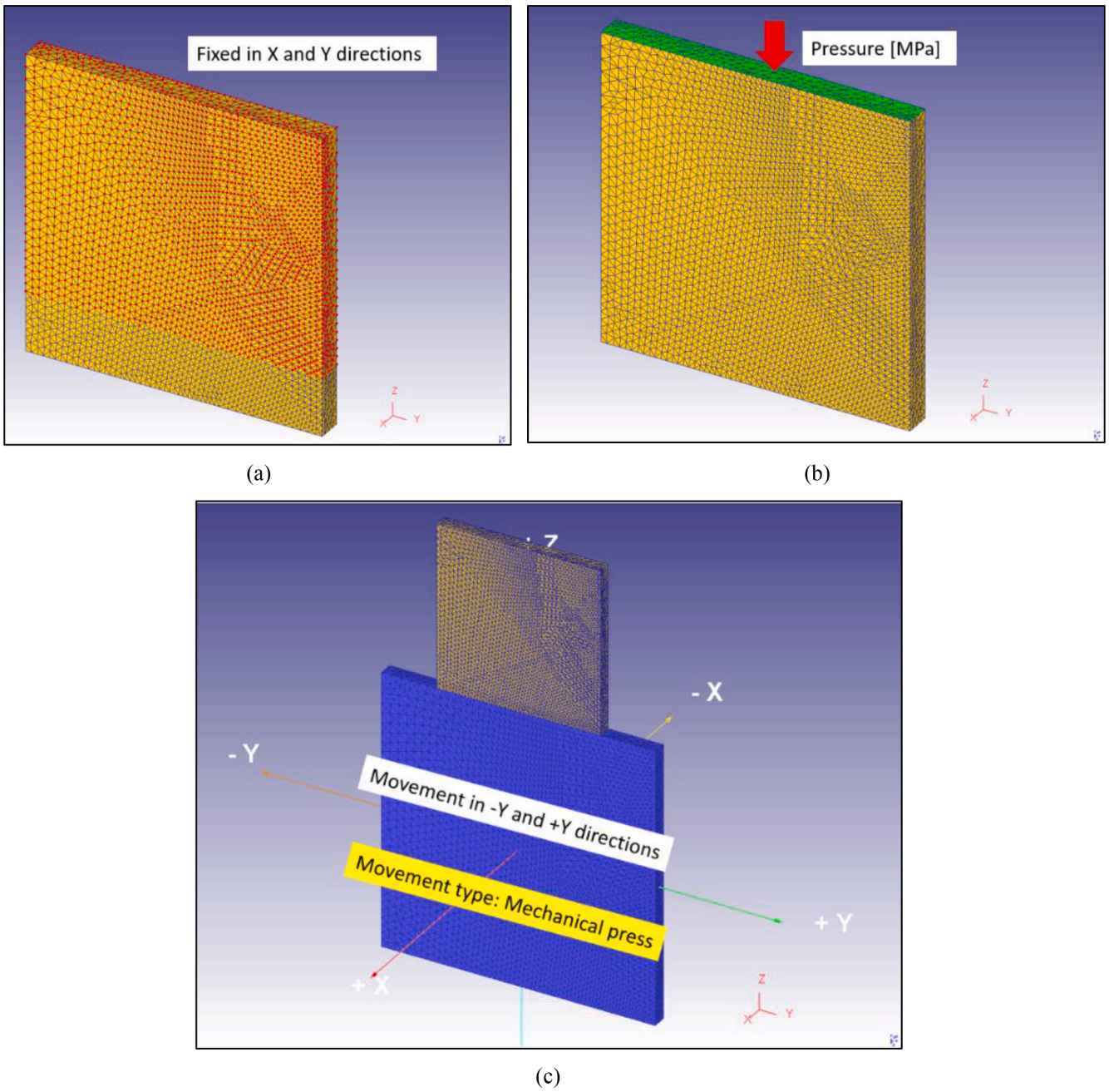

Fig. 1. The loads and boundary conditions of (a) the lower workpiece, (b) the upper workpiece, and (c) the assembly and movement of the workpieces.

2017; Masoumi, 2018).

A common point among most of the above studies, is the identification of grain size change, as one of the most important microstructural factors, that determines the subsequent mechanical properties of the welded joint (Dalgård, 2011; Chamanfar, 2013). On the other hand, the transition from laboratory scale to industrial size components requires the determination of the critical LFW process parameters and their impact on grain size evolution. Such determination will allow for the design of optimum LFW conditions in order to achieve reliable and consistent properties of the weld joint. The most important fundamental mechanism that governs the evolution of the grain size during a thermomechanical process, such as LFW, is the recrystallization. In the case of LFW, dynamic recrystallization (DRX), i.e., recrystallization occurring during deformation, is the main mechanism. In this context, in recent years, the development of microstructure-based finite element (FE) simulation models has become of great interest to many researchers; however, very few works have quantified the impact of LFW process parameters on the occurrence and extent of dynamic recrystallization in a LFW joint. The data is even more scarce when it comes to LFW of superalloys. Such data is of critical importance for the development of industrial size LFWed components for the hot section of aircraft engines (Blisks made for turbine section).

Ceretti et al. (2010) developed a 2D FE model using DEFORM™ software to predict the temperature gradients evolution during the LFW of AISI 1045 steel. However, the influence of LFW process parameters on grain size changes was not modelled, predicted, or optimized. Fratini et al. (2012) carried out an experimental investigation on the effect of the LFW parameters including oscillation frequency and applied pressure on the final average grain size (AGS) during the LFW of an ASTM A285 steel. They also developed a 3D FE model using DEFORM™ software to analyze the influence of the LFW parameters on temperature distribution. The experimental measurements demonstrated that the

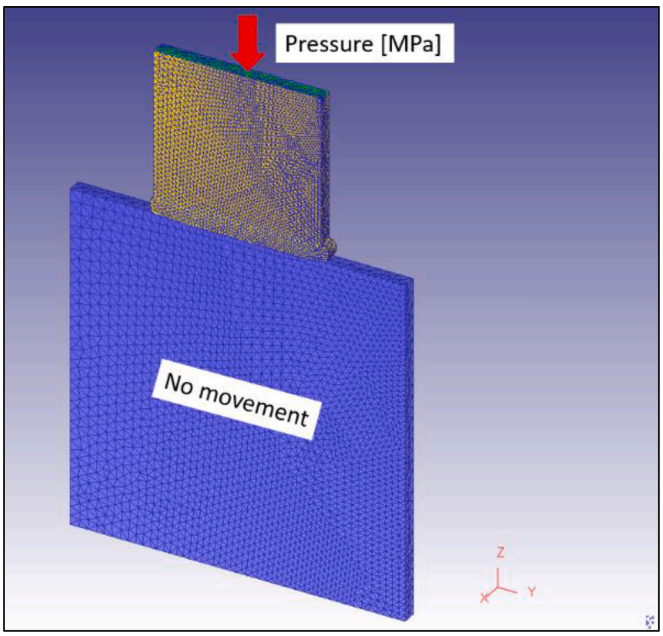

Fig. 2. The loads and boundary conditions of the upper and lower workpieces in the forging/cooling step.

Table 1
Mechanical, thermal, and material properties of Waspaloy (38).

Properties	Waspaloy
Density $\rho\,(kg/m^3)$	8200
Young's modulus $E\,(MPa)$	$E(T)$
Poisson's ratio υ	0.3
Thermal conductivity $k\,(W/m^oC)$	$k(T)$
Specific heat capacity $c\,(J/kg^oC)$	$C_p(T)$
Thermal expansion coefficient $\alpha\,(1/^oC)$	$\alpha(T)$

average grain diameter increased from the weld line to the parent material. The numerical analysis also showed that the smallest selected value of oscillation frequency provided insufficient heat, resulting in poor welds. However, the evolution of the AGS was not predicted and optimized.

McAndrew et al. (2015) experimentally and numerically investigated the impact of the LFW parameters on average interface force, friction coefficient and temperature distribution in LFW of Ti-6Al-4 V alloy. DEFORM™ was used to develop a 3D FE model. The results showed that the above-mentioned outputs were considerably dependent on the oscillation frequency and applied pressure. Buffa et al. (2015) measured and predicted the temperature distribution for different oscillation frequencies and applied pressures during LFW of AA2011-T3 alloy. The experimental measurements and numerical predictions using DEFORM™ were well matched. Bühr et al. (2018) developed a FE model of LFW of Ti–6Al–4 V using Abaqus® software to predict the interface temperature. They found that the interface temperature decreased when a higher pressure was applied and the workpieces oscillated along the smaller dimension of the interface surfaces. In none of the above two studies, however, the grain size evolution as a function of process parameters was not discussed.

Bagheri et al. (2020) numerically studied the influence of vibrations on temperature, heat generation, and mechanical properties during a FSW process with different welding speeds. In addition, they observed that the measured grain size and simulated temperature of the FSVW-ed sample were, respectively, finer and larger than those of the FSW-ed sample. Abbasi et al. (2021) analyzed the grain topology, grain size distribution, average grain size, and the dynamic recrystallization fraction numerically and experimentally. The results demonstrated that the temperature in friction-stir-vibration (FSV) welded samples were higher than that in friction-stir (FS) welded specimens. They also found that the grain size of the weld area decreased when the vibration was applied during friction stir welding. Furthermore, the workpiece vibration in the FSV produced higher deformation in the material compared to the FS, resulting in higher DRX and finer grains.

Bagheri et al. (2022) optimized the friction stir welding (FSW) parameters for joining AA6061-T6 aluminum alloys using the Taguchi method and statistical analysis. They also modeled the FSW process using Abaqus® software to verify the results obtained from the experimental analysis. They found that the grain size of the stir zone under optimal welding parameters (6–8 μm) was finer than that of non-optimal welding parameters (11–13 μm). Abdollahzadeh et al. (2023) studied the pinless friction stir spot welding of aluminum-copper composite with Zn interlayer using experiments and simulations. The FE results obtained by Abaqus® showed that the temperature decreased from top to bottom in the direction of the thickness. Bagheri et al. (2023) investigated microstructural, thermal, and mechanical properties of Al/SiC/Cu composites fabricated by 50 nm and 250 nm SiC particles by friction stir spot welding. Moreover, they studied the temperature distribution and mechanical characteristics of the composite with different nanoparticle sizes using Abaqus®. The results indicated that large reinforcing particles increased the temperature and grain size in the stir zone of the joint sample.

The above review of the literature shows that although temperature evolution during LFW has been measured and simulated, the impact of LFW process parameters on AGS evolution has not been quantified and predicted based on a microstructure-based evolution model considering the occurrence of dynamic recrystallization. In the present research, a FE model is developed for the LFW of Ni-base superalloy Waspaloy that allows predicting weld joint grain sizes based on the JMAK model using the DEFORM™. The predictions of the FE model were validated using experimental data published in the literature. In addition, using a statistical analysis based on design of experiments (DoE) and analysis of variance (ANOVA), the most effective LFW parameters on peak temperature (PT) and AGS were identified. Then, the regression models of PT and AGS were developed and the optimal LFW parameters were determined based on single-criterion optimization of AGS and multi-criteria optimization of AGS and PT to reduce PT and AGS using the hill-climbing technique.

Table 3
LFW parameters utilized for FE validations (Chamanfar et al., 2011)

Run No.	LFW parameters $a(mm)$	$f\,(HZ)$	$P\,(MPa)$
A	3	80	70
B	3	80	90

Table 2
The Johnson-Cook material constants of Waspaloy (Dong et al., 2020)

$A\,(MPa)$	$B\,(MPa)$	n	C	m	$\dot{\varepsilon}_0(1/s)$	$T_{melt}\,(^oC)$	$T_{room}\,(^oC)$
520	622	0.6522	0.0134	1.3	0.01	1500	20

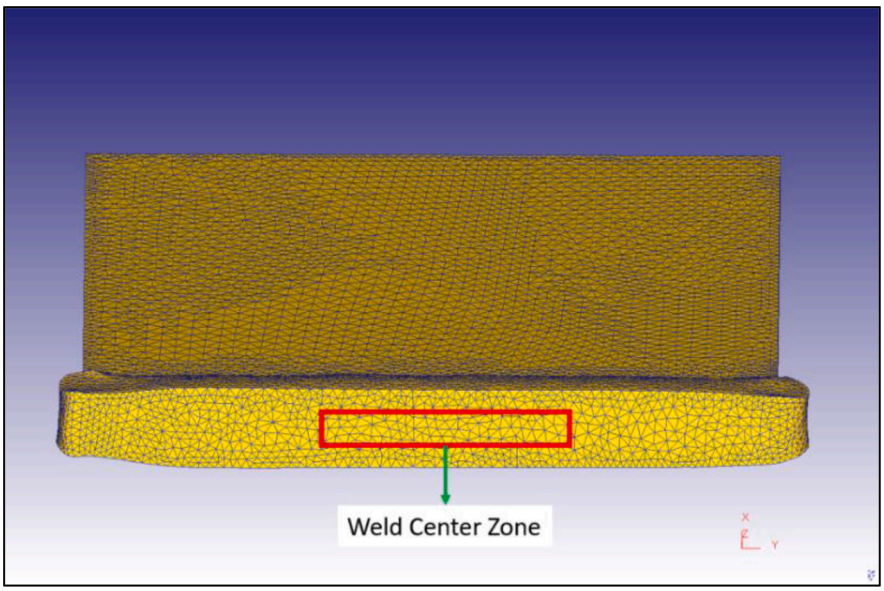

Fig. 3. Weld interface center zone for AGS and PT extraction in the FE simulations.

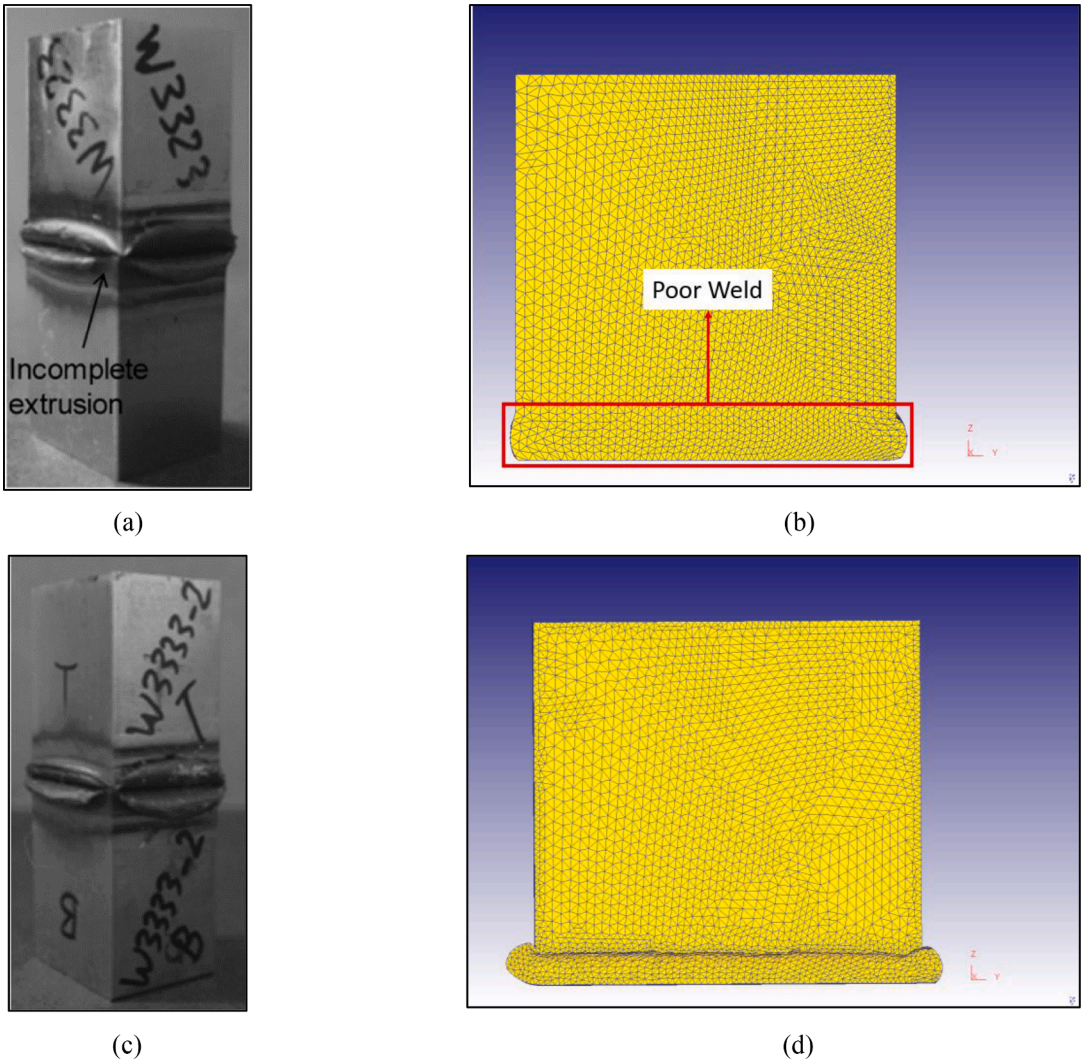

Fig. 4. Experimental and numerical final welds of test No. A (a (Chamanfar et al., 2011) and b) and test No. B (c (Chamanfar et al., 2011) and d).

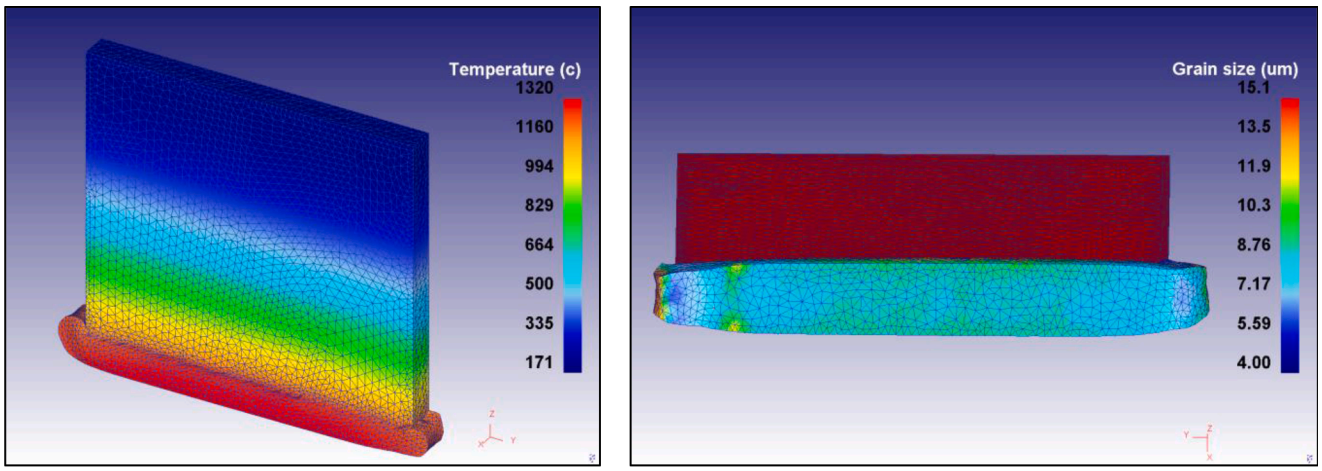

Fig. 5. The FE predicted (a) temperature and (b) grain size.

Table 4
The calibrated frictional and thermal coefficients in the FE models

Shear Friction Factor, m	0.95
Heat Transfer Coefficient, h_{int} $[N/sec^{-1}/mm^{-1}/^{\circ}C^{-1}]$	11
Heat Convection Coefficient, h $[N/sec^{-1}/mm^{-1}/^{\circ}C^{-1}]$	0.02

Table 5
LFW parameters using D-optimal DoE and the FE predicted average grain sizes and peak temperatures

Run No.	LFW parameters (Input)			Responses (Output)	
	$a(mm)$	f (HZ)	P (MPa)	d_{avg} (μm)	T_p (^oC)
1	3.5	80	90	9.9	1320
2	3.5	100	161	6.1	1400
3	3.1	70	134	6.8	1350
4	2.5	88	134	6.4	1330
5	3.5	70	200	3.5	1390
6	2.5	70	200	3.5	1400
7	2.9	100	154	6.1	1380
8	2.9	100	90	9.7	1330
9	2.5	100	200	3.8	1420
10	2.5	70	90	10.3	1300
11	3.1	88	200	3.9	1400

FE simulations of linear friction welding and microstructure alterations

The LFW process can be modeled based on two approaches namely Heat-Transfer Analysis and Thermo-Mechanical Analysis. In the first approach, only temperature is considered and no displacement is included in the model. Therefore, the workpieces are stationary. In the second approach, both displacements and temperature are considered, and therefore, oscillation of a part against the other could be considered in the simulations, which is more representative of the actual LFW process. Furthermore, the two workpieces can be modeled as Deformable / Rigid Bodies, Deformable / Deformable Bodies, or Single Body.

In the present research work, the Thermo-Mechanical Analysis approach with Deformable / Rigid Bodies was used (Bertrand et al., 2018; Li et al., 2010). Although this approach is less accurate than Deformable / Deformable Bodies, it has been frequently used in the previous works (Buffa et al., 2015; Buffa et al., 2016; Kiselyeva et al., 2012; Turner et al., 2011; Yamileva et al., 2012). This approach is proper for industrial applications because it can be more easily applied with considerably lower computational cost and faster convergence. In addition, due to the symmetry of the process, only one deformable body is considered to simulate LFW process (Buffa et al., 2015; Buffa et al., 2016; Kiselyeva et al., 2012; Turner et al., 2011; Yamileva et al., 2012).

A 3D thermo-mechanical finite element model based on updated Lagrangian formulation was developed using the DEFORM™-3D software. The lower and upper workpieces and the applied mesh and boundary conditions in the LFW model are shown in Figs. 1 and 2. The lower workpiece was modeled as a rigid object with about 50,000 tetrahedral elements (Fig. 1a), while the upper workpiece was considered as a thermo-visco-plastic object and meshed with 100,000 tetrahedral elements (Fig. 1b). An adaptive remeshing algorithm was used and a mesh window was allocated to the workpiece to have a high-quality fine mesh at the weld interface.

To reproduce the experimental LFW process in the simulations, the following constraints were applied to the movement of the workpieces: (1) the oscillation motion in the horizontal direction (Y) was applied to the lower workpiece and a constant pressure was applied on the top surface of the upper workpiece (Figs. 1b and c); (2) the lower workpiece was fixed in the vertical direction (Z) and the upper workpiece was fixed in both the X and Y directions (Figs. 1a and c); (3) no boundary condition was allocated to the upper workpiece's nodes close to the contact zone to allow flash formation during the LFW process (Fig. 1a); (4) the oscillation was removed and a forge pressure equal to the applied pressure during oscillation was applied to the upper workpiece (Fig. 2). This stabilization process is called the forging step.

The mechanical contact between the lower and upper workpieces was modeled using the shear friction model as follows:

$$\tau = m\tau_{flow} \tag{1}$$

where m is the shear friction coefficient and τ_{flow} is the shear flow stress at the interface of the upper and lower workpieces. The shear friction coefficient was calibrated by comparing the simulated AGS and PT with the corresponding experimental results. The thermal contact between the upper and lower workpieces was applied at the contact surface using the heat conduction during the LFW process as:

$$Q = h_{int}(T_{UW} - T_{LW}) \tag{2}$$

where h_{int} is the heat transfer coefficient, T_{UW} and T_{LW} are the temperatures of the upper and lower workpieces. The heat transfer coefficient was calibrated experimentally. Moreover, convection heat transfer was considered between the workpieces and the ambient as follows:

$$Q = h(T_{WP} - T_a) \tag{3}$$

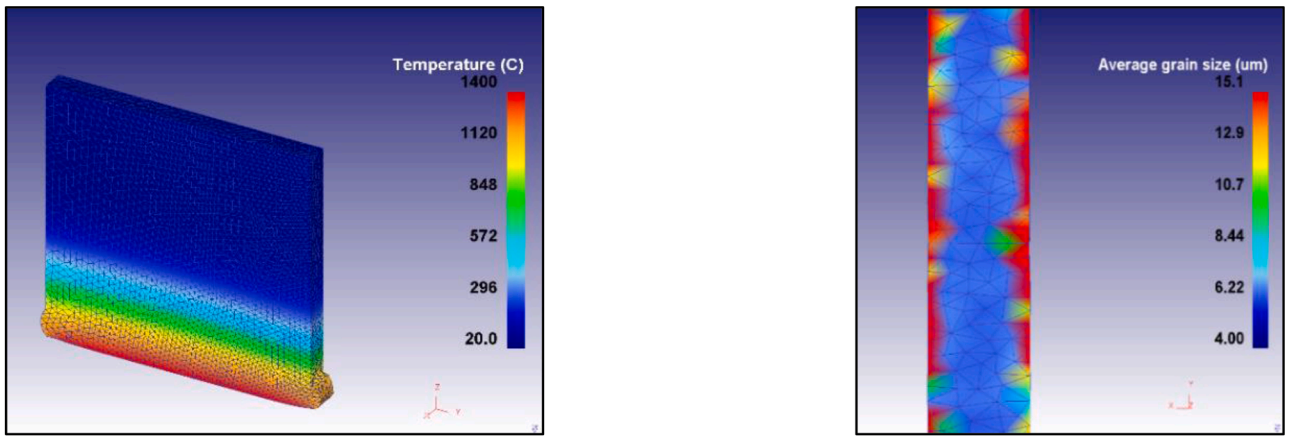

Fig. 6. The FE predicted average grain sizes and temperatures for Test Nos. 2, 6, 9, and 11.

in which h is the convection heat transfer coefficient, and T_{WP} and T_a are the workpiece and ambient (room) temperatures.

The Johnson-Cook material constitutive model was used to model the thermo-visco-plastic deformation of the workpiece material as follows:

$$\sigma_{fl} = [A + B(\varepsilon)^n]\left[1 + C\ln\left(\frac{\dot{\varepsilon}}{\dot{\varepsilon}_0}\right)\right]\left[1 - \left(\frac{T - T_{room}}{T_{melt} - T_{room}}\right)^m\right] \quad (4)$$

where σ_{fl} is the flow stress of the workpiece material, ε is the plastic strain, $\dot{\varepsilon}$ the plastic strain rate (s^{-1}), $\dot{\varepsilon}_0$ the reference plastic strain rate (s^{-1}), $T(^{\circ}C)$ the workpiece temperature, T_{melt} $(^{\circ}C)$ the melting temperature of the workpiece, and $T_{room}(^{\circ}C)$ the room temperature. Moreover, A (MPa) is the initial yield strength, B (MPa) the hardening modulus, C the strain rate sensitivity coefficient, n the hardening coefficient, and m the thermal softening coefficient. Both workpieces were made of

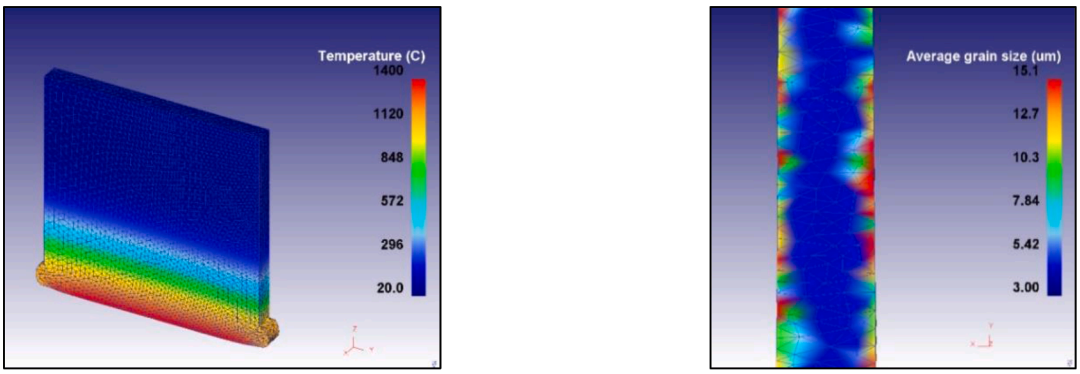

Fig. 6. (*continued*).

Table 6
ANOVA for prediction of regression models of grain size and peak temperature

Predictor	d_{avg} (μm)		T_p (^oC)	
	Coef.	P-value	Coef.	P-value
Intercept	13.9944		1142.871	
a	0.1638	0.6563	10.6795	0.2475
f	0.0033	0.7732	0.8143	0.0178
P	-0.0558	< 0.0001	0.8102	< 0.0001
Model		< 0.0001		< 0.0001
	Fit Statistics		*Fit Statistics*	
R^2	97.74%		94.6%	
R^2_{adj}	96.78%		92.29%	
R^2_{Pred}	94.34%		87.59%	
Adequate Precision	22.39		16.71	

Table 7
Validation tests

Run No.	LFW parameters		
	a(*mm*)	*f* (*HZ*)	*P* (*MPa*)
12	2.6	75	120
13	3.3	95	180

Waspaloy, whose mechanical, thermal, and material properties are presented in Table 1 and the Johnson-Cook material constants of Waspaloy are listed in Table 2.

The Avrami recrystallization model available in the DEFORM^{TM} software was used to simulate the AGS (DEFORM, 2017, Sadeghifar et al., 2020). The modules of Static, Meta-dynamic, and Dynamic Recrystallizations, and Grain Growth were used to predict AGS (Huang et al., 2001, Loyda et al., 2016, Reyes et al., 2016). The temperature, strain, strain rate, activation energies and initial grain size are the input parameters into the FE model. Using the JMAK model, peak strain (ε_P), dynamic recrystallized volume fractions (X_{DRx}), dynamic recrystallized grain size (d_{DRx}), and average grain size (d_{avg}) were predicted. Dynamic recrystallization takes place when a critical strain ε_c is reached. The critical strain is a function of the peak strain ε_p, i.e. $\varepsilon_c = a_2(\varepsilon_p)$, where a_2 is an Avrami constant (DEFORM, 2017, Sadeghifar et al., 2020, Huang et al., 2001, Loyda et al., 2016, Reyes et al., 2016):

$$\varepsilon_p = a_1 d_0^{h_1} \dot{\varepsilon}^{m_1} \exp(Q_{act} m_1 / RT) + c_1 \tag{5}$$

where R is the gas constant, Q_{act} is the activation energy, a_1, h_1, m_1, and c_1 are material constants. The dynamic recrystallization and the fraction of dynamically recrystallized grains are given based on the Avrami equation as (DEFORM, 2017, Sadeghifar et al., 2020, Huang et al., 2001, Loyda et al., 2016, Reyes et al., 2016):

$$X_{DRx} = 1 - \exp\left[-\beta_d \left(\frac{\varepsilon - a_{10}\varepsilon_p}{\varepsilon_{0.5}} \right)^{k_d} \right] \tag{6}$$

in which ε is the strain, ε_p is the peak strain, and X_{DRx} is the volume fraction of dynamically recrystallized material. $\varepsilon_{0.5}$ is the strain for X_{DRx}= 0.5, which is formulated as:

$$\varepsilon_{0.5} = a_5 d_0^{h_5} \dot{\varepsilon}^{n_5} \dot{\varepsilon}^{m_5} \exp(Q_{act} m_5 / RT) + c_5 \tag{7}$$

where d_0 is the initial diameter of the grains, and a_5, h_5, n_5, m_5, and c_5 are the Avrami material constants. The dynamically recrystallized grain size is calculated by (DEFORM, 2017, Sadeghifar et al., 2020, Huang et al., 2001, Loyda et al., 2016, Reyes et al., 2016):

$$d_{DRx} = a_8 d_0^{h_8} \dot{\varepsilon}^{n_8} \dot{\varepsilon}^{m_8} \exp(Q_{act} m_8 / RT) + c_8 \tag{8}$$

where a_8, h_8, n_8, m_8, and c_8 are the Avrami material constants. AGS is obtained using the mixture rule as:

$$d_{avg} = d_0(1 - X_{DRx}) + d_{DRx} X_{DRx} \tag{9}$$

An initial AGS of d_0=15.1 μm, which was measured by Ref. (Chamanfar et al., 2011), was used for FE predictions.

Validation of the finite element model

The developed 3D finite element model was validated by comparing the predicted AGS and PT at the weld interface with the experimental ones measured by the same research group (Chamanfar et al., 2011). Rectangular blocks were prepared by electro-discharge machining (EDM) from an as-received Waspaloy disc. LFW was conducted by applying the oscillation using an MTS LFW Process Development System (PDS, MTS Systems Corporation, Eden Prairie, MN). This system has one in-plane actuator that oscillates the lower workpiece in the horizontal direction and one forge actuator that applies a downward force on the upper workpiece (Chamanfar et al., 2011). A Chromel Alumel K type thermocouple was used to measure the temperature during the LFW process. The grain size was measured using electron backscatter diffraction (EBSD) (Chamanfar et al., 2011).

As displayed in Table 3, two LFW test conditions (A and B) presented in Ref. (Chamanfar et al., 2011) were used for FE validations. In the present research work, the grain sizes were simulated using the JMAK constants of Waspaloy in DEFORM^{TM} library (Dalgaard et al., 2009). It is worth mentioning here that the values of AGS and PT after and before forging/cooling step, respectively, were extracted and averaged from the weld interface center zone, as shown in Fig. 3. In addition, although all the recrystallization modes were implemented into the model, the simulated grain size in the weld interface zone was mostly affected by the DRX mode. This was also reported by Chamanfar et al. (Chamanfar

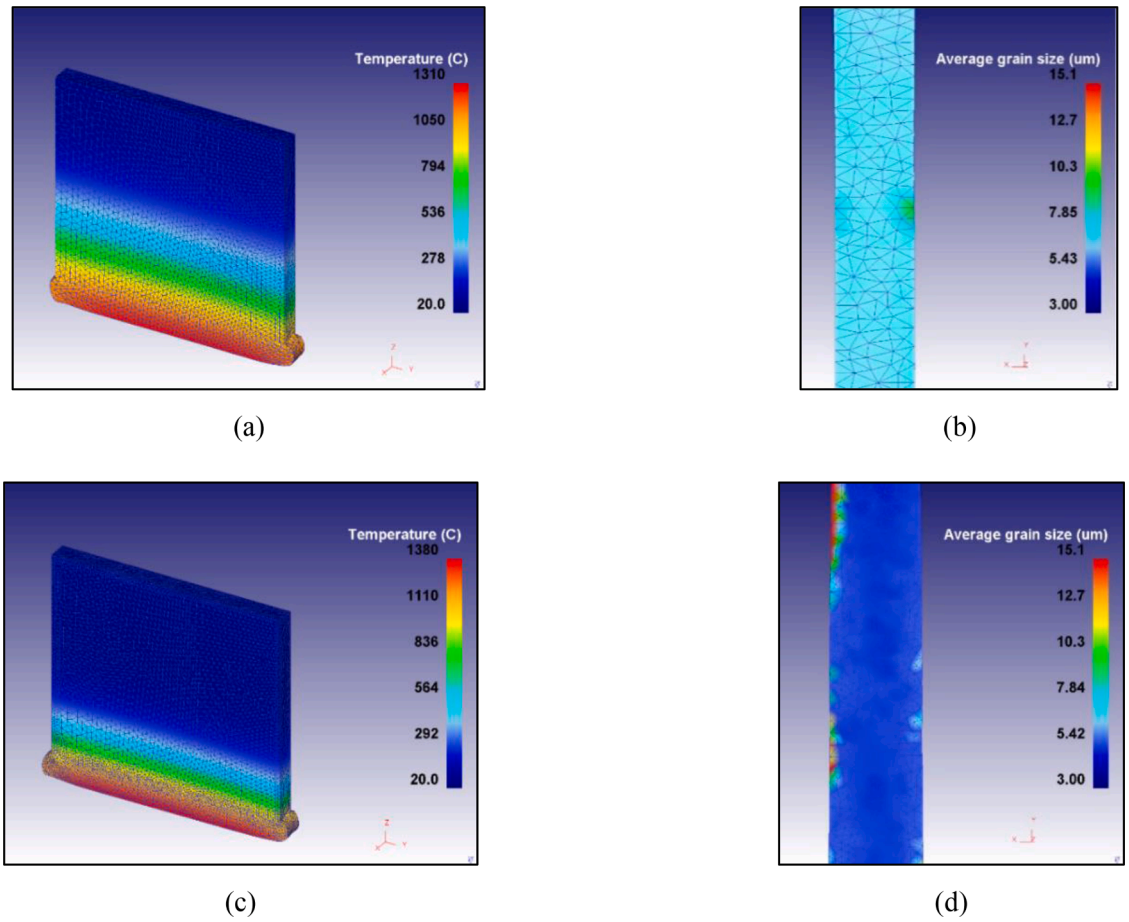

Fig. 7. The FE results of temperatures and average grain sizes for test No. 12 (a and b) and test No. 13 (c and d).

Table 8
FE simulations and regression predictions for validation of regression models

	FE Simulation		Regression Prediction	
Run No.	d_{avg} (μm)	T_p (^oC)	d_{avg} (μm)	T_p (^oC)
12	7.2	1310	7.9	1328.93
13	5.1	1380	4.8	1401.3

Table 9
The optimum solution for average grain size

$a(mm)$	f (HZ)	P (MPa)	d_{avg} (μm)
2.5	70	200	3.5

et al., 2011), where DRX operated during the LFW of Waspaloy at the interface and its proximity. As seen in Fig. 4, poor and complete welds were observed for both experimental and numerical LFW processes for Tests A and B. According to Ref. (Chamanfar et al., 2011), the poor weld was created due to different temperature distributions on each side of the interface and a greater extrusion of the plasticized and softened layer of the upper workpiece. In addition, the extruded material was not extended to all the corners in the poorly welded specimens because bonding was not entirely integral at the interface due to the formation of micro voids.

The predicted (Fig. 5) and measured (Chamanfar et al., 2011) PT were 1320 and 1280 °C, respectively. The predicted (Fig. 5) and measured (Chamanfar et al., 2011) AGS were equal to 8.1 and 7.5 μm, respectively. Thus, good agreement was observed between the predicted and measured AGS and PT for Test B. This was achieved by exploring various magnitudes of shear friction and heat transfer coefficients and choosing appropriate ones using the calibration of the simulation results with the experiments, as shown in Table 4.

Design of Experiments and Response Surface Method

The LFW simulations were conducted using the D-optimal design of experiments (DoE). Eleven LFW parameters were generated in the DoE using the Design-Expert® software. The independent factors were oscillation amplitude, oscillation frequency, and applied pressure. Response surface method (RSM) was used to find a suitable approximation to the output quantities in terms of input variables (Montgomery, 2017). A complete linear model was utilized as indicated in Eq. (10):

$$y = b_0 + b_1 a + b_2 f + b_3 P \tag{10}$$

where b_0 to b_3 are the regression coefficients.

The coefficient of determination, R^2, was calculated as (2):

$$R^2 = 1 - (SSE / SST) \tag{11}$$

in which $SSE = \sum_{i=1}^{n} (y_i - \hat{y}_i)^2$ and $SST = \sum_{i=1}^{n} (y_i - \bar{y})^2$, where y_i is the true output response, here obtained from the experiments, $\hat{y}_i$ is the approximate response computed from RSM, $\bar{y}$ is the average of the true response, n is the number of design points used to generate the model, and i is the number of independent variables in the model.

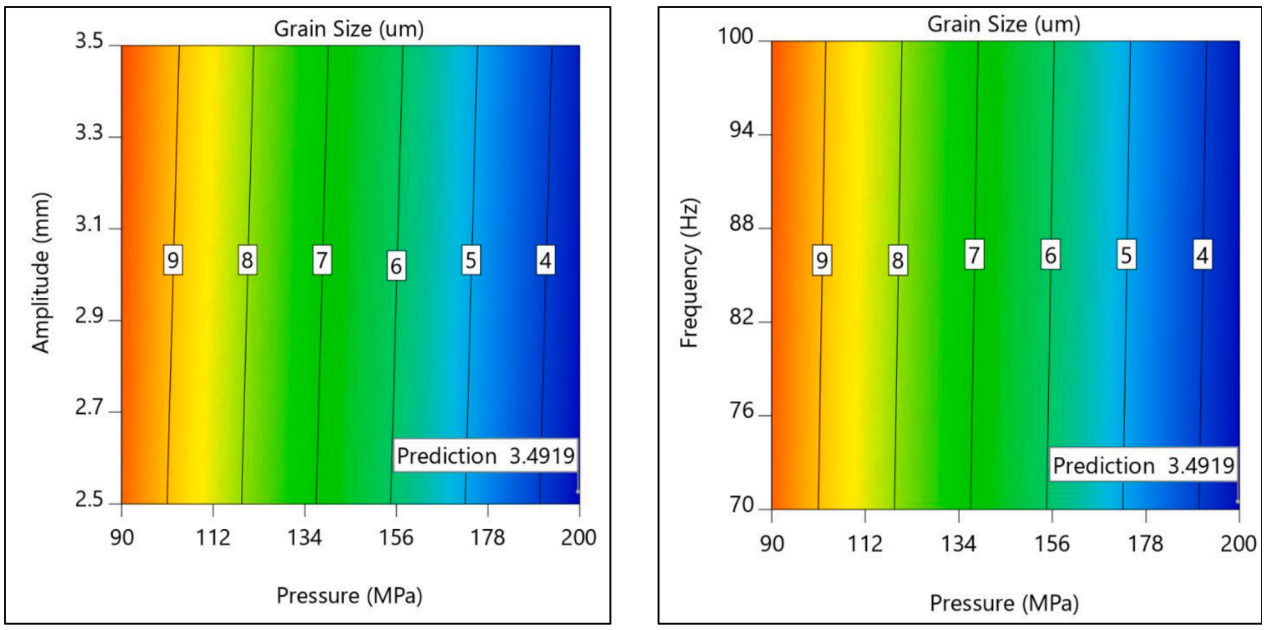

Fig. 8. The variation of average grain size with pressure, oscillation amplitude, and oscillation frequency.

Table 10
Weighting coefficients (importance) of the individual objective functions for multi-criteria optimization of AGS and temperature

Case	w_{AGS}	w_T
I	0.3	0.3
II	0.5	0.3
III	0.3	0.5

Table 11
The optimum solutions for average grain size and peak temperature for three cases

Case	$a(mm)$	$f\ (HZ)$	$P\ (MPa)$	$d_{avg}\ (\mu m)$	$T_p\ (^oC)$
I	2.5	70	158	5.8	1355
II	2.5	70	178	4.7	1371
III	2.5	70	138	6.9	1338

Single-criterion and multi-criteria optimization formulations

Using the response function of the AGS (d_{avg}) obtained in the previous section, the SC optimization is formulated as follows:

$$\begin{gathered} Finda, f, andPto \\ Minimized_{avg} \\ Subjecttoa_L - a \le 0, a - a_U \le 0, f_L - f \le 0, \\ f - f_U \le 0, P_L - P \le 0, andP - P_U \le 0 \end{gathered} \tag{12}$$

where a, f, and P are the design variables, d_{avg} is the objective function, and a_L, f_L, and P_L and a_U, f_U, and P_U are the lower and upper bounds of the design variables, respectively.

In addition, the MC optimization formulation is presented for AGS and PT (T_p) below:

$$\begin{gathered} Finda, f, andPto \\ Minimized_{avg} and T_p \\ Subjecttoa_L - a \le 0, a - a_U \le 0, f_L - f \le 0, \\ f - f_U \le 0, P_L - P \le 0, andP - P_U \le 0 \end{gathered} \tag{13}$$

where d_{avg} and T_p are the objective functions. The optimization was based on a hill-climbing technique using a penalty approach.

Results and discussions

A comparative analysis of grain size and peak temperature

Table 5 provides the predicted AGS and PT in terms of LFW parameters for Test Nos. 1 to 11. The simulated AGS and temperatures of Test Nos. 2, 6, 9, and 11 are shown in Fig. 6. As reported in Table 5, the smallest AGS occurred at Test Nos. 5 and 6 equal to 3.5 μm. The above two tests correspond to the largest value of contact pressure equal to 200 *MPa*. It is also seen that the largest magnitude of AGS occurred at Test No. 10, where the minimum values of oscillation amplitude, oscillation frequency, and contact pressure were used. This might be attributed to the fact that a high contact pressure generates large friction at the interface of the lower and upper workpieces and a larger contact area, producing high frictional heat, which leads to a smaller AGS.

The lowest PT occurred at Test No. 10, in which the minimum values of oscillation amplitude, oscillation frequency, and pressure were utilized. In contrast, the highest magnitude of PT was observed at Test No. 9, where oscillation frequency and pressure were maxima. This is because a large oscillation frequency brings along a high strain rate that increases the flow stress of the material, which produces a larger plastic work and consequently a larger heat generation and temperature. In addition, a high contact pressure generates a large friction at the interface of the lower and upper workpieces and a larger contact area, which can produce high frictional heat and larger temperatures. On the other hand, both a large oscillation frequency and contact pressure leads to a larger flow velocity and more material extrusion toward the edges of the contact surface, Therefore, more heat can evacuate and the temperature may decrease faster (Ji et al., 2016). In a LFW process, there is a competition between these phenomena, depending on the magnitudes of the oscillation frequency and contact pressure. In the present simulation, the first phenomenon dominates the LFW process.

Analysis of Variance and regression modelling

The numerical results of AGS and PT were used to derive the pre-

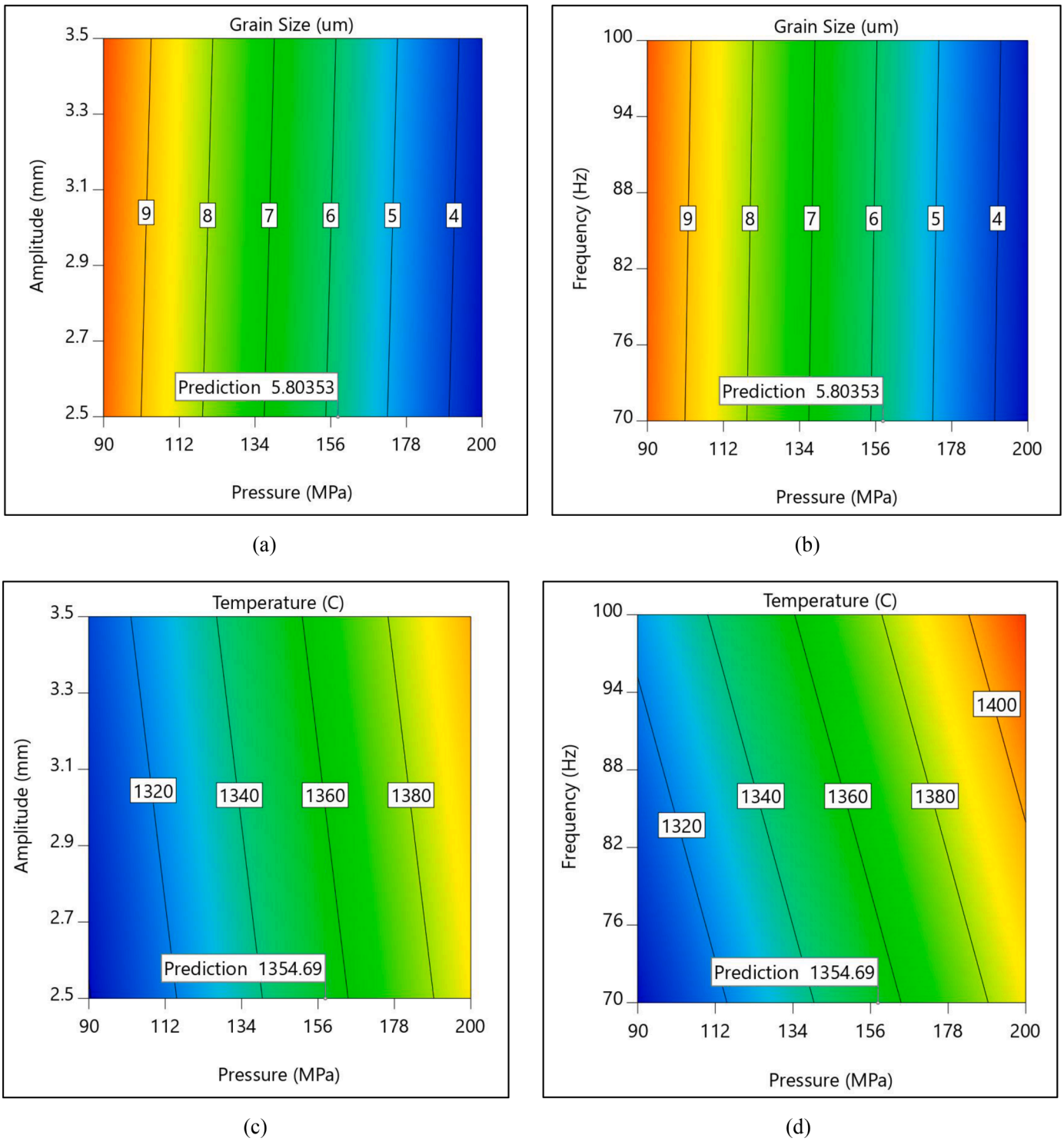

Fig. 9. The variation of peak temperature and average grain size with pressure, oscillation amplitude, and oscillation frequency for Case I.

dictive mathematical linear models using RSM. The predicted regression models were utilized to determine the influence of LFW parameters on AGS and PT using ANOVA. The regression coefficients of each predictive model are shown in Table 6. This table also presents the ANOVA results to quantify the significance and the accuracy of the regression models (*P-value*, R^2, R^2_{adj}, R^2_{Pred}, and Adequate Precision) of LFW parameters. The regression parameters with *P* values less than 0.05 were considered to be Significant in the predictive models according to the variance analyses at a 95% confidence (Effertz et al., 2019). It needs to be mentioned that the regression models are more accurate when R^2, R^2_{adj}, and R^2_{Pred} are closer to 1. Adequate Precision determines the signal-to-noise ratio, in which a ratio greater than 4 is desirable.

As presented in the ANOVA results in Table 6, the *P-value* of the regression models was smaller than 5%, demonstrating that all the models are Significant. Since R^2, R^2_{adj}, and R^2_{Pred} magnitudes are between 87% and 97%, the models could be considered statistically precise (Sadeghifar et al., 2020) and can be used with a high level of confidence to predict AGS and PT in the design space given in the DoE. The R^2, R^2_{adj},

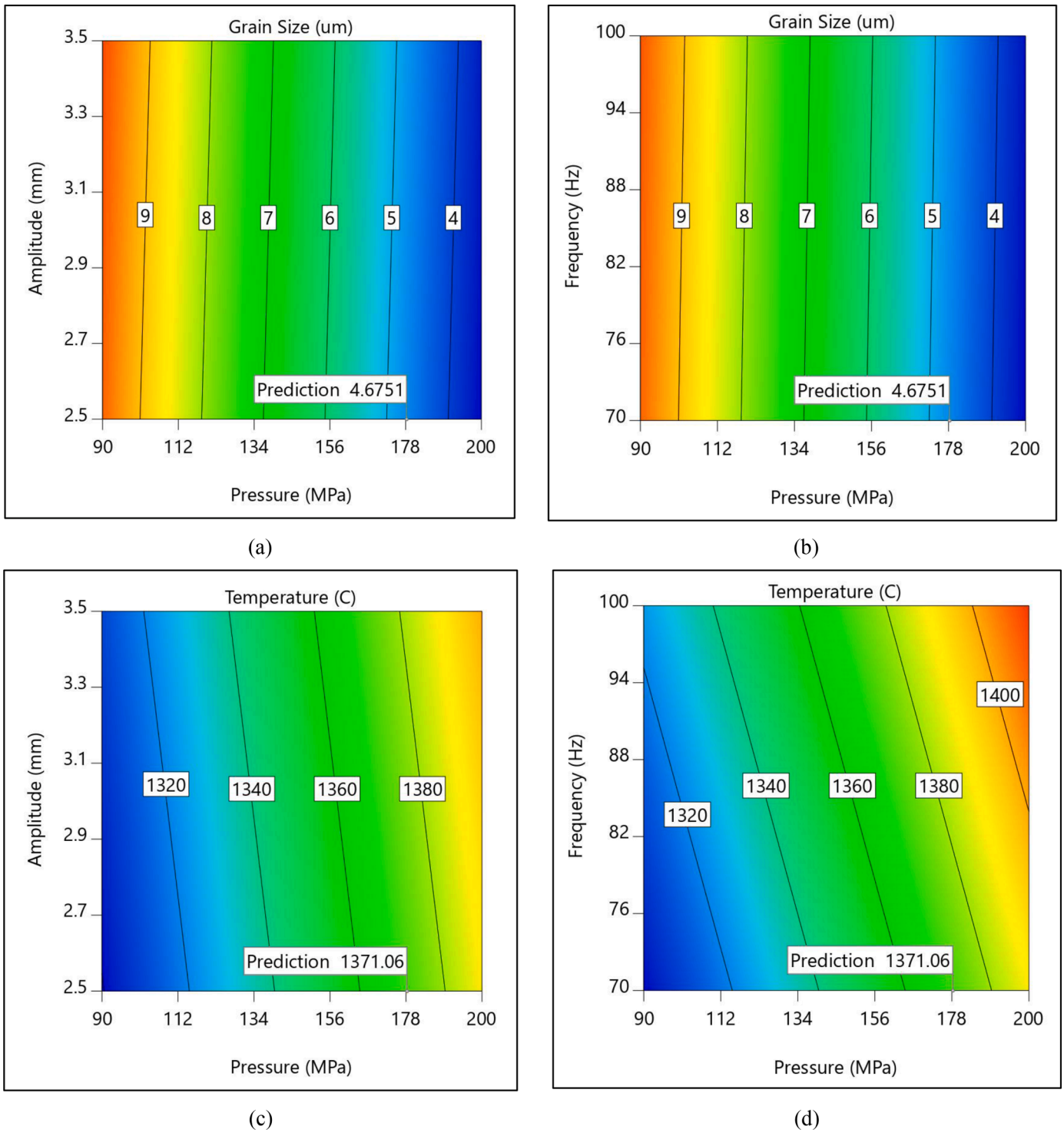

Fig. 10. The variation of peak temperature and average grain size with pressure, oscillation amplitude, and oscillation frequency for Case II.

and R^2_{Pred}values are between 94% and 97% for AGS and between 87% and 94% for PT, showing the models are reliable. Based on the ANOVA results shown in Table 6, pressure is the most significant parameter affecting AGS and PT, which is confirmed by the results of previous studies (Fratini et al., 2012, Ji et al., 2016, McAndrew et al., 2018, McAndrew et al., 2015, Tabaie et al., 2021). Oscillation amplitude and frequency have almost the same effect on AGS, while oscillation frequency is more influential than oscillation amplitude on temperature. The same result was reported by (Fratini et al., 2012, Ji et al., 2016, McAndrew et al., 2018, McAndrew et al., 2015).

Validation of the predictive regression model

As displayed in Table 7, two extra LFW tests (Nos. 12 and 13) were selected in the space of the design of experiment in order to validate the regression models. The predicted AGS and PT using the regression models for test Nos. 12 and 13 were calculated using Eqs. (14-17). Moreover, the FE simulated AGS and temperature for the above-mentioned tests were illustrated in Fig. 7. The FE simulated AGS and temperatures for Run Nos. 12 and 13 were compared with those predicted using the regression equations in Table 8. As seen in this table,

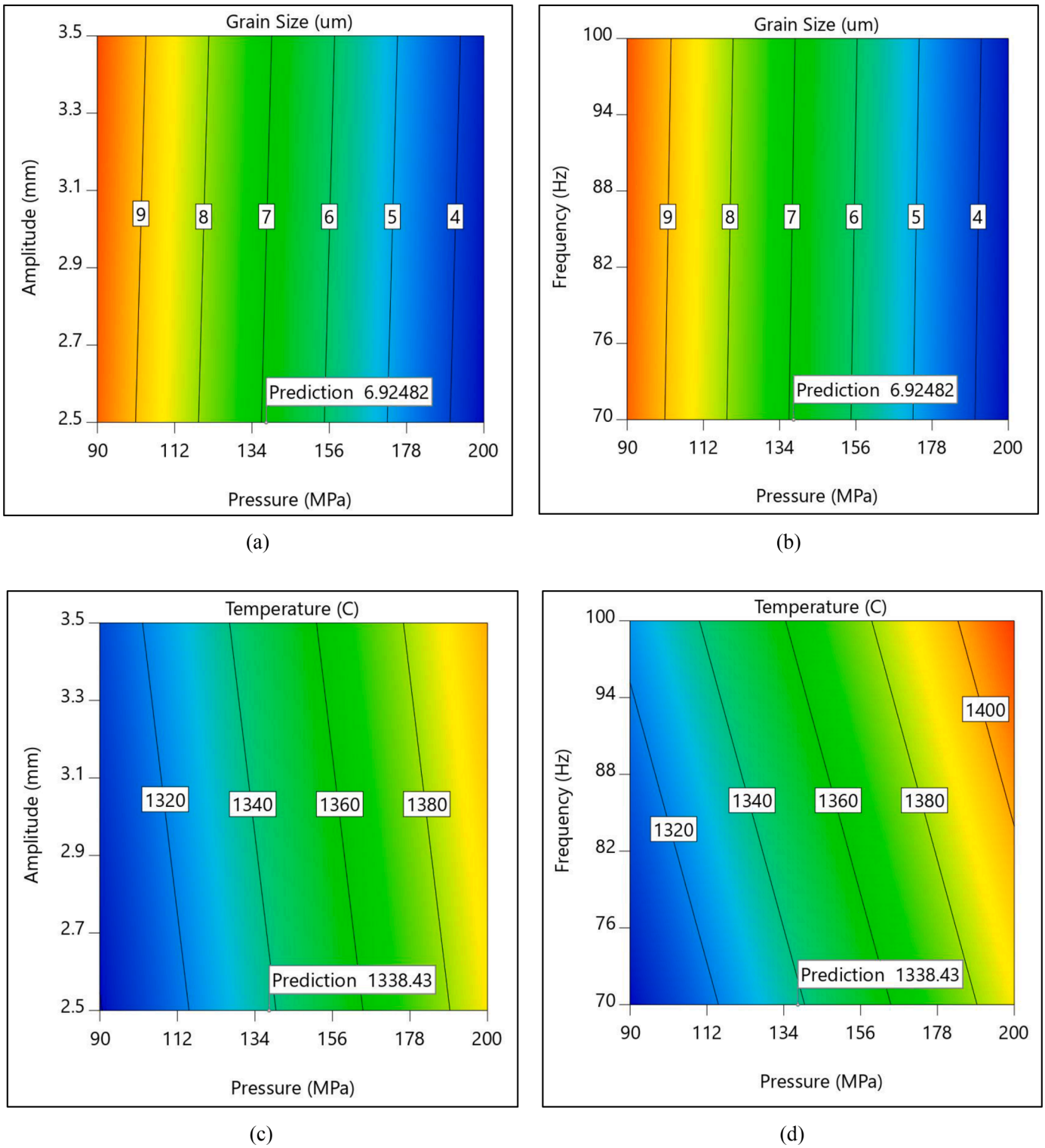

Fig. 11. The variation of peak temperature and average grain size with pressure, oscillation amplitude, and oscillation frequency for Case III.

there is good agreement between the FE simulations and regression predictions. Accordingly, the developed regression models are precise and can be used to predict AGS and PT induced by the LFW process in the space of design of experiment.

$$\textbf{RunNo.12}: d_{avg}\ (a=2.6, f=75, P=120) = 13.9944 + 0.1638\,a + 0.0033\,f - 0.0558\,P = 7.97 \quad (14)$$

$$\textbf{RunNo.13}: d_{avg}(a=3.3, f=95, P=180) = 13.9944 + 0.1638a + 0.0033f - 0.0558P = 4.8 \quad (15)$$

$$\textbf{RunNo.12}: T_p\ (a=2.6, f=75, P=120) = 1142.871 + 10.6795\,a + 0.8143\,f + 0.8102\,P = 1328.93 \quad (16)$$

$$\textbf{RunNo.13}: T_p\,(a=3.3, f=95, P=180) = 1142.871 + 10.6795\,a + 0.8143\,f + 0.8102\,P = 1401.3 \quad (17)$$

Single-criterion optimization of AGS

As listed in Table 9, the optimum oscillation amplitude, oscillation frequency, and pressure were obtained as 2.5 *mm*, 70 *HZ*, and 200 *MPa*, respectively. In addition, the optimized value of AGS was 3.489 μm. The optimized AGS was the same as its smallest value in the 11 design points in the DoE. Therefore, both ANOVA and optimization results showed that the smallest oscillation amplitude and oscillation frequency and the largest pressure in the design space led to the lowest AGS.

Fig. 8 also shows the variation of AGS with pressure, amplitude, and frequency in the optimization process. As seen in this figure, AGS is mostly dependent on pressure.

Multi-criteria optimization of AGS and PT

Three configurations of the total objective function based on different weighting coefficients, whose values are given in Table 10, are studied. The objective was to minimize both AGS and PT with different importance in order to increase the material strength (McAndrew et al., 2018, Sadeghifar et al., 2020) and decrease the LFW-induced residual stresses (McAndrew et al., 2018), respectively. The optimization results given in Table 11 showed that for Case II, in which the weighting coefficient (importance) of AGS is higher than that of PT, the smallest grain size was obtained for the pressure of 178 *MPa* while PT was higher than that in the other cases. For Case III, where the weighting coefficient of PT was larger, the lowest PT was achieved for the pressure of 138 *MPa* while AGS was smaller than that in Cases I and II. For Case I, in which the weighting coefficients of AGS and PT are the same, AGS and PT converged to medium values compared with Cases II and III.

Figs. 9, 10, and 11 show the variation of AGS and PT with pressure, amplitude, and frequency in the optimization process. As seen in these figures, both AGS and PT are more dependent on pressure than oscillation amplitude and oscillation frequency.

Summary and conclusions

In the present research, a 3D FE model of LFW of Waspaloy was developed to predict AGS and temperature based on the JMAK recrystallization model using the DEFORM^{TM} software. The LFW parameters include oscillation amplitude, oscillation frequency, and applied pressure. The FE model was validated using the experimental AGS previously measured by the same research group. Although all the recrystallization modes including Dynamic, Meta-Dynamic, Static Recrystallizations, and Grain Growth were considered in the FE model, the DRX mode mainly dominated the predicted average grain size in the weld interface zone. The D-optimal method was used to create the DoE for FE simulations. The RSM and ANOVA demonstrated that the AGS and PT were mostly affected by the applied pressure. Moreover, the effects of oscillation amplitude and frequency were almost the same on AGS. The influence of oscillation frequency on temperature was more than oscillation amplitude. The statistical analysis showed that the P-value of the regression models was smaller than 5% and R^2, R^2_{adj}, and R^2_{Pred} were between 87% and 97%, which revealed that the predictive regression models of PT and AGS were precise and reliable. To validate the regression models, two extra LFW tests were selected in the space of the DoE. The SC optimization results demonstrated that the smallest oscillation amplitude (2.5 mm) and oscillation frequency (70 HZ) and the highest applied pressure (200 MPa) in the range of the DoE produced the minimum AGS (3.489 μm). The MC optimum values showed that both AGS and PT are more dependent on pressure. The finite element and regression models can be utilized as a predictive tool for the design of joining conditions of industrial size components with tailored microstructures, which thereby minimize expensive and time-consuming experimental measurements.

Declaration of Competing Interest

The authors declare that they have no known competing financial interests or personal relationships that could have appeared to influence the work reported in this paper.

Data availability

The authors do not have permission to share data.

References

Abbasi, M., Bagheri, B., Sharifi, F., 2021. Simulation and experimental study of dynamic recrystallization process during friction stir vibration welding of magnesium alloys. Trans. Nonferr. Metals Soc. China 31 (9), 2626–2650.

Abdollahzadeh, A., Bagheri, B., Vaneghi, A.H., Shamsipur, A., Mirsalehi, S.E., 2023. Advances in simulation and experimental study on intermetallic formation and thermomechanical evolution of Al–Cu composite with Zn interlayer: effect of spot pass and shoulder diameter during the pinless friction stir spot welding process. In: Proceedings of the Institution of Mechanical Engineers, Part L: Journal of Materials: Design and Applications, 237, pp. 1475–1494.

Bagheri, B., Abdollahzadeh, A., Abbasi, M., Kokabi, A.H., 2020. Numerical analysis of vibration effect on friction stir welding by smoothed particle hydrodynamics (SPH). Int. J. Adv. Manufact. Technol. 110, 209–228.

Bagheri, B., Shamsipur, A., Abdollahzadeh, A., Mirsalehi, S.E., 2023. Investigation of SiC nanoparticle size and distribution effects on microstructure and mechanical properties of Al/SiC/Cu composite during the FSSW process: experimental and simulation. Metals Mater. Int. 29 (4), 1095–1112.

Bagheri, B., Sharifi, F., Abbasi, M., Abdollahzadeh, A, 2022. On the role of input welding parameters on the microstructure and mechanical properties of Al6061-T6 alloy during the friction stir welding: experimental and numerical investigation. In: Proceedings of the Institution of Mechanical Engineers, Part L: Journal of Materials: Design and Applications, 236, pp. 299–318.

Bertrand, S., Shahriari, D., Jahazi, M., Champliaud, H., 2018. Linear friction welding process simulation of Ti-6Al-4V alloy: a heat transfer analysis of the conditioning phase. Proced. Manufact. 15, 1382–1390.

Bhamji, I., Preuss, M., Threadgill, P.L., Moat, R.J., Addison, A.C., Peel, M.J., 2010. Linear friction welding of AISI 316L stainless steel. Mater. Sci. Eng. A 528 (2), 680–690.

Buffa, G., Cammalleri, M., Campanella, D., Fratini, L., 2015. Shear coefficient determination in linear friction welding of aluminum alloys. Mater. Des. 82, 238–246.

Buffa, G., Cammalleri, M., Campanella, D., La Commare, U., Fratini, L., 2017. Linear friction welding of dissimilar AA6082 and AA2011 aluminum alloys: microstructural characterization and design guidelines. Int. J. Mater. Form. 10, 307–315.

Buffa, G., Campanella, D., D'annibale, A., di Ilio, A., Fratini, L., 2014. Experimental and numerical study on linear friction welding of AA2011 aluminum alloy. In: Key Engineering Materials, 611. Trans Tech Publications Ltd, pp. 1511–1518.

Buffa, G., Campanella, D., Pellegrino, S., Fratini, L., 2016. Weld quality prediction in linear friction welding of AA6082-T6 through an integrated numerical tool. J. Mater. Process. Technol. 231, 389–396.

Bühr, C., Colegrove, P.A., McAndrew, A.R., 2018. A computationally efficient thermal modelling approach of the linear friction welding process. Journal of Mater. Process. Technol. 252, 849–858.

Ceretti, E., Fratini, L., Giardini, C., La Spisa, D., 2010. Numerical modelling of the linear friction welding process. Int. J. Mater. Form. 3 (1), 1015–1018.

Chamanfar, A., 2013. Evolution of Microstructure and Mechanical Properties in Linear Friction Welded Waspaloy (Doctoral Dissertation. McGill University.

Chamanfar, A., Jahazi, M., Cormier, J., 2015. A review on inertia and linear friction welding of Ni-based superalloys. Metall. Mater. Trans. A 46, 1639–1669.

Chamanfar, A., Jahazi, M., Gholipour, J., Wanjara, P., Yue, S., 2011. Mechanical property and microstructure of linear friction welded WASPALOY. Metall. Mater. Trans. A 42 (3), 729–744.

Chamanfar, A., Jahazi, M., Gholipour, J., Wanjara, P., Yue, S., 2013. Modeling grain size and strain rate in linear friction welded Waspaloy. Metall. Mater. Trans. A 44 (9), 4230–4238.

Dalgaard, E., Jahazi, M., Merati, A., Wanjara, P., 2009. Mechanical Properties of Linear Friction Welded Ti-6-4V Alloy. American Institute of Aeronautics and Astronautics, pp. 1416–1424.

Dalgård, E.C., 2011. Evolution of microstructure, microtexture, and Mechanical Properties in Linear Friction Welded Titanium Alloys (Doctoral Dissertation. McGill University.

Deform, 2017. DEFORM Software, Version 11.2. DEFORM Software, Columbus, Ohio, USA.

Desin Design-Expert User's Manual, Version 12, 2019.

Dong, L., Wang, J., Zhu, X., Zhang, S., Li, T., Li, K., 2020. Study on the law of wear of milling cutter for Waspaloy internal threads with a small diameter. Int. J. Adv. Manufact. Technol. 107 (3), 1327–1336.
Effertz, P.D.S., Fuchs, F., Enzinger, N., 2019. The influence of process parameters in linear friction welded 30CrNiMo8 small cross-section: a modelling approach. Sci. Technol. Weld. Joining 24 (2), 121–129.
Fratini, L., Buffa, G., Campanella, D., La Spisa, D., 2012. Investigations on the linear friction welding process through numerical simulations and experiments. Mater. Des. 40, 285–291.
Fu, Y., Li, W.Y., Yang, X.W., 2015. Microstructure analysis of linear friction welded AISI 321 stainless steel joint. J. Eng. Sci. Technol. Rev. 8, 37–39.
Huang, D., Wu, W.T., Lambert, D., Semiatin, S.L., 2001. Computer simulation of microstructure evolution during hot forging of Waspaloy and nickel alloy 718. Minerals. Metals Mater. Soc./AIME, Microstr. Model. Predict. During Thermomech. Process. (USA) 137–146.
Ji, S., Wang, Y., Liu, J., Meng, X., Tao, J., Zhang, T., 2016. Effects of welding parameters on material flow behavior during linear friction welding of Ti6Al4V titanium alloy by numerical investigation. Int. J. Adv. Manufact. Technol. 82 (5), 927–938.
Kiselyeva, S.K., Yamileva, A.M., Karavaeva, M.V., Nasibullayev, I.S., Bychkov, V.M., Medvedev, A.Y., Supov, A.V., Musin, F.F., Alexandrov, I.V., Latysh, V.V., 2012. Computer modelling of linear friction welding based on the joint microstructure. J. Eng. Sci. Technol. Rev. 5, 44–47.
Li, W., Wang, F., Shi, S., Ma, T., Li, J., Vairis, A., 2014. 3D finite element analysis of the effect of process parameters on linear friction welding of mild steel. J. Mater. Eng. Perform 23, 4010–4018.
Li, W.Y., Ma, T., Li, J., 2010. Numerical simulation of linear friction welding of titanium alloy: effects of processing parameters. Mater. Des. 31 (3), 1497–1507.
Li, Y., Liu, Y., Liu, C., Li, C., Ma, Z., Huang, Y., Li, W., 2018. Microstructure evolution and mechanical properties of linear friction welded S31042 heat-resistant steel. J. Mater. Sci. Technol. 34 (4), 653–659.
Loyda, A., Hernández-Muñoz, G.M., Reyes, L.A., Zambrano-Robledo, P., 2016. Microstructure modeling of a Ni-Fe-based superalloy during the rotary forging process. J. Mater. Eng. Perform. 25, 2128–2137.
Ma, T.J., Li, W.Y., Xu, Q.Z., Zhang, Y., Li, J.L., Yang, S.Q., 2008. Linear friction welding of Ti-6Al-4V alloy: microstructure characterization. In: Materials Science Forum, 580. Trans Tech Publications Ltd, pp. 405–408.
Ma, T.J., Zhong, B., Li, W.Y., Zhang, Y., Yang, S.Q., Yang, C.L., 2012. On microstructure and mechanical properties of linear friction welded dissimilar Ti–6Al–4V and Ti–6· 5Al–3· 5Mo–1· 5Zr–0· 3Si joint. Sci. Technol. Weld. Joining 17 (1), 9–12.
Masoumi, F. (2018). Evolution of microstructure and mechanical properties during linear friction welding of AD730 TM Ni-based superalloy (Doctoral dissertation, École de technologie supérieure).
McAndrew, A.R., Colegrove, P.A., Addison, A.C., Flipo, B.C., Russell, M.J., 2015a. Modelling the influence of the process inputs on the removal of surface contaminants from Ti–6Al–4V linear friction welds. Mater. Design (1980-2015) 66, 183–195.
McAndrew, A.R., Colegrove, P.A., Addison, A.C., Flipo, B.C., Russell, M.J., Lee, L.A., 2015b. Modelling of the workpiece geometry effects on Ti–6Al–4V linear friction welds. Mater. Des. 87, 1087–1099.
McAndrew, A.R., Colegrove, P.A., Bühr, C., Flipo, B.C., Vairis, A., 2018. A literature review of Ti-6Al-4V linear friction welding. Prog. Mater. Sci. 92, 225–257.
Montgomery, D.C., 2017. Design and Analysis of Experiments. John wiley & sons.
Reyes, L.A., Páramo, P., Salas Zamarripa, A., de la Garza, M., Guerrero-Mata, M.P., 2016. Influence of processing parameters on grain size evolution of a forged superalloy. J. Mater. Eng. Perform. 25, 179–187.
Sadeghifar, M., Javidikia, M., Songmene, V., Jahazi, M., 2020. Finite element simulation-based predictive regression modeling and optimum solution for grain size in machining of Ti6Al4V alloy: influence of tool geometry and cutting conditions. Simul. Modell. Pract. Theory 104, 102141.
Schroeder, F., Ward, R.M., Turner, R.P., Attallah, M.M., Gebelin, J., Reed, R.C., Walpole, A.R., 2012. Linear friction welding of titanium alloys for aeroengine applications: modelling and validation. In: 9th International Conference on Trends in Welding Research, pp. 886–892.
Sivaraj, P., Vinoth Kumar, M., Balasubramanian, V., 2019. Microstructural characteristics and tensile properties of linear friction-welded AA7075 aluminum alloy joints. In: Advances in Materials and Metallurgy: Select Proceedings of ICEMMM 2018. Springer, Singapore, pp. 467–476.
Smith, M., Levesque, J.B., Bichler, L., Sediako, D., Gholipour, J., Wanjara, P., 2017. Residual stress analysis in linear friction welded in-service Inconel 718 superalloy via neutron diffraction and contour method approaches. Mater. Sci. Eng. A 691, 168–179.
Tabaie, S., Rézaï-Aria, F., Flipo, B.C., Jahazi, M., 2021. Grain size and misorientation evolution in linear friction welding of additively manufactured IN718 to forged superalloy AD730™. Mater. Charact. 171, 110766.
Turner, R., Gebelin, J.C., Ward, R.M., Reed, R.C., 2011. Linear friction welding of Ti–6Al–4V: modelling and validation. Acta Mater. 59, 3792–3803.
Vishwakarma, K.R., Ojo, O.A., Wanjara, P., Chaturvedi, M.C., 2014. Microstructural analysis of linear friction-welded 718 plus superalloy. Jom 66, 2525–2534.
Yamileva, A.M., Yuldashev, A.V., Nasibullayev, I.S., 2012. Comparison of the parallelization efficiency of a thermo-structural problem simulated in SIMULIA Abaqus and ANSYS mechanical. J. Eng. Sci. Technol. Rev. 5, 39–43.